Nuclear Instruments and Methods in Physics Research A 755 (2014) 69–77

Contents lists available at ScienceDirect

Nuclear Instruments and Methods in Physics Research A

journal homepage: www.elsevier.com/locate/nima

GLORIA: A compact detector system for studying heavy ion reactions using radioactive beams

G. Marquínez-Durán [a], L. Acosta [a], R. Berjillos [a], J.A. Dueñas [a], J.A. Labrador [a,b], K. Rusek [c], A.M. Sánchez-Benítez [a,d], I. Martel [a,*]

[a] Department of Applied Physics, University of Huelva, 21071 Huelva, Spain
[b] National Accelerator Centre, University of Seville, 41092 Seville, Spain
[c] Heavy Ion Laboratory, University of Warsaw, 02-093 Warsaw, Poland
[d] GSI Helmholtzzentrum fur Schwerionenforschung GmbH, D-64291 Darmstadt, Germany

ARTICLE INFO

Article history:
Received 8 July 2013
Received in revised form
31 March 2014
Accepted 3 April 2014
Available online 18 April 2014

Keywords:
Heavy ions
Silicon detector array
Double-sided silicon strip detector
Direct nuclear reactions
Radioactive beams
Nuclear astrophysics

ABSTRACT

In this paper we describe a compact and large solid-angle silicon array, the **GLO**bal **R**eact**I**on **A**rray (GLORIA), designed to study direct nuclear reactions induced by exotic nuclei at energies close to the Coulomb barrier. The detector array consists of six particle-telescopes arranged in a very close geometry around a 30° rotated-target system, allowing for the measurement of reaction fragments in a continuous angular range from 15° to 165° (Lab). GLORIA has been used for first time at the SPIRAL/GANIL facility at Caen (France) to study the scattering of the system ^{8}He+^{208}Pb at the collision energies of 16 and 22 MeV.

1. Introduction

In recent years the physics developed at radioactive beam facilities [1,2] has provided several exciting results concerning the understanding of fundamental nuclear physics and astrophysics. The usually low beam intensities and the variety of reaction fragments of interest, quite often produced in very small quantities, make necessary the use of particle detectors with large solid angle and angular coverage. These detectors must provide efficient particle identification capabilities as well as a wide energy range of operation, a large and continuous angular coverage, good energy resolution and high granularity for angular correlation measurements.

Silicon detectors present excellent characteristics for detecting heavy ions at moderate counting rates (few kHz/cm^2) due to their high detection efficiency and good energy resolution. Moreover, using the present technology it is possible to manufacture Double-Sided Silicon Strip Detectors (DSSSD) with small strip pitch (<100 μm) and a large active area ($>60\times60$ mm^2) [3]. Therefore they have become widespread devices for the construction of the charged particle detector arrays needed at radioactive beam facilities.

A number of silicon detector arrays such as MUST2 [4,5] and TIARA [6] have been built over the last years mainly dedicated to the study of nuclear reactions with light targets in inverse kinematics. The new silicon detector array, GLORIA, is foreseen for the detection of reaction fragments produced in direct reactions with heavy targets at energies around the Coulomb barrier.

GLORIA has been designed with a very compact geometry able to fit in a small volume of 20 cm diameter. A dedicated rotated target configuration avoids the unwanted shading of detectors due to the target ladder and the target foil itself. The DSSSD detectors are fixed to a dedicated mechanical structure providing overlapping angular regions (10° Lab) between particle telescopes. Altogether, the system allows for obtaining a full angular distribution of the physical quantities in the range from 15° to 160° (Lab). By the use of two-stage DSSSD telescopes of 40 μm and 1 mm thickness, the new detector array is expected to resolve mass and ion charge up to carbon isotopes. This silicon array could also be used together with gamma detection systems like EXOGAM [7] or AGATA [8], as well as with compact mass spectrometers like VAMOS [9] for detailed gamma-particle experiments. The GLORIA detector has been first used at GANIL laboratory (Caen, France) for studying the scattering of ^{8}He on ^{208}Pb at energies around the Coulomb barrier.

In this paper we discuss the main features of GLORIA detector and its performance using radioactive beams. Detailed Monte

* Corresponding author.
E-mail address: imartel@uhu.es (I. Martel).

http://dx.doi.org/10.1016/j.nima.2014.04.002
0168-9002/

Carlo simulations are compared with preliminary experimental results for the scattering of ^{8}He on ^{208}Pb at 22 MeV (Lab).

2. Design of the detector array

Several requirements were imposed during the designing process:

- Angular resolution. At Coulomb barrier energies the cross-sections for relevant processes present slow variation with the scattering angle θ, and therefore a maximum value of $\delta\theta = \pm 2.5^{\circ}$ (Lab) was adopted. The expected beam spot size of a typical experiment is about 3 mm. DSSSD detectors with a strip pitch of 3 mm are widely available at reasonable cost and therefore this option was a convenient choice for our design.
- Angular range. Close to the Coulomb barrier, breakup fragments are expected to dominate at forward angles, whereas the transfer channels will extend to the backward region. Measurement of the elastic channel at very forward angles is also important for normalization purposes. Continuous angular range coverage between 15° and 165° (Lab) should be achieved while keeping a close distance to the reaction target in order to maximize the solid angle.
- A beam entrance/exit aperture of 14 mm diameter was implemented for driving the beam trough the detector array. This opening is sufficient for most of the low energy radioactive beam facilities.
- Detector geometry. The detectors should be fixed to a dedicated mechanical structure to reduce systematic uncertainties. Angular overlapping regions between adjacent telescopes were studied in order to provide a continuous angular distribution. An angular overlap of 10° Lab between detectors was chosen for this purpose.
- Symmetry considerations. Reflection symmetry of the configuration with respect to the reaction plane (up/down, left/right, backward/forward) would be a clear advantage for data analysis, as it would allow for the comparison of pixel counting rates at symmetric positions with respect to the beam axis. In this way, systematic uncertainties arising from mechanical misalignments and target non-uniformities could be corrected.
- Energy resolution. Typical energy resolution of DSSSD detectors is around 30 keV. In the case of thin 40 μm DSSSD detectors, silicon thickness can vary as much as 5% along detector's surface, which affects the final energy resolution of the telescope. Additional energy degradation of the system is due to the effect of target thickness and beam spot size. Therefore, a proper pixel-by-pixel energy calibration procedure was implemented in the analysis programme.
- "Plug & Play" concept. GLORIA detector was designed to be used at radioactive beam facilities elsewhere, so an easy experimental setup and transportation system have been considered in the mechanical design.

The final configuration of GLORIA is shown in Fig. 1. The detector array consists of six two-stage particle telescopes. Two pairs of telescopes are placed covering forward and backward angles, whereas the other two are placed above and below the target, respectively. The telescopes, which are mechanically fixed to a compact stainless steel frame, are oriented in such a way that the centre of the surface of the first stage (ΔE) is tangent to a sphere of 60 mm radius around the centre of the array. Each telescope is made of a first stage DSSSD (ΔE) of 40 mm thickness, and a second DSSSD (E) of 1 mm thickness. In this configuration the angular range covered by a single telescope is close to 45°, keeping the required angular overlap of 10° between adjacent telescopes.

The DSSSD detectors are based on the model W1 (DS) type 9G delivered by Micron Semiconductor [3]. They are totally depleted doubled-sided DC silicon strip detectors. In this particular model the standard Aluminium layer has been replaced by a metallic grid, which occupies only 3% of the total active area, improving the lower energy detection limit.

These detectors are fabricated on 4-in. technology, having 16 junction elements (X position) and another 16 ohmic elements (Y position). Detector elements (strips) have a total length of 49.5 mm, 3 mm width and an inter-strip pitch of 100 μm. The detector has a total surface of 50×50 mm^2, resulting altogether in 256 pixels of 9 mm^2 area. The wafer is packaged in the standard FR4 transmission frame allowing for assembling several silicon layers in dE/E configuration for particle identification. The double X–Y segmentation provides heavy-ion impact-position information and thus the scattering angle. Target frame and telescopes are fixed to the same structure and therefore the angular uncertainty is mainly dominated by the pixel geometry and the beam spot size at the reaction target. With the present configuration a geometrical angular resolution of $\pm 2.5^{\circ}$ (Lab) can be achieved with spot sizes up to 4 mm diameter and a beam divergence around 1°. A suitable collimation system was designed to keep optimal working conditions at low energy radioactive beam facilities (see Section 3).

The supporting structure has been manufactured in stainless steel 4 mm thick, providing enough rigidity to the system at a reasonable low weight (< 500 g). The structure is placed on

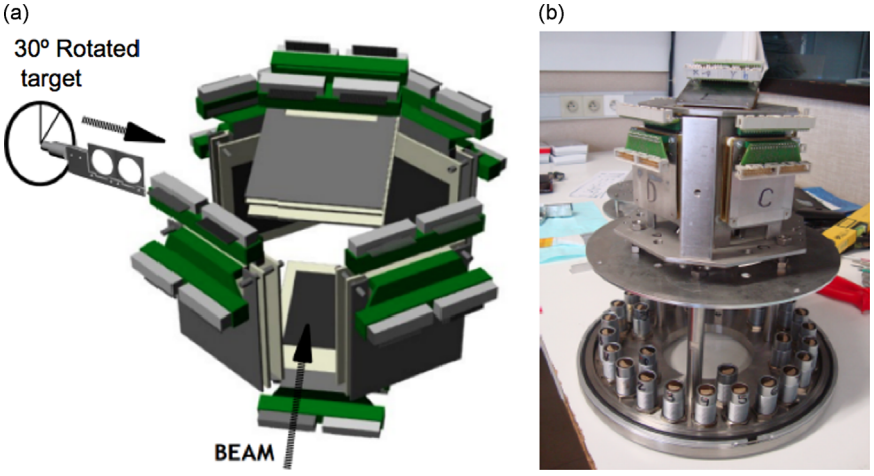

Fig. 1. (a) Geometry of telescopes and rotated target frame. (b) Supporting structure is fixed to an ISO 250 flange. See the text for discussion.

a supporting plate for adjusting the X, Y and Z positions (± 10 mm, respectively) relative to the DN 250 LF flange, which was then coupled to the vacuum chamber. The telescopes are fixed to the outer side of the mechanical structure, making possible the addition of further silicon stages and/or thick scintillator detectors. Each DSSSD detector produces 32 independent signals, which together with the needed grounding gives a total of $32 \times 12 = 384$ electronic channels. The flange is provided with 25 LEMO high-vacuum feed-troughs (18-channels each), two per detector plus an extra one dedicated to the connections of auxiliary beam-tuning equipment.

The target ladder enters horizontally into the detector array, and it should be rotated 30° with respect to the vertical plane for optimal operation (Fig. 1). This target positioning avoids the shading of the detectors that otherwise would produce the target and its frame. In this way it becomes possible the measurement of cross-sections around 90°.

3. Reaction chamber and beam diagnostic systems

Fig. 2 shows a sketch of GLORIA reaction chamber together with the corresponding beam diagnostic elements. The mechanical structure is mounted in a dedicated reaction chamber, a six way cross DN250 with ISO-K type clamp flange connections for vacuum sealing. Typical vacuum level of 10^{-7} mb is obtained after five hours of pumping, which is already sufficient for opening the system to the accelerator beam line. At the entrance and exit of the reaction chamber there are three four-way DN-100 crosses accommodating beam diagnostic systems (S1, S2 and S3 in Fig. 2), two of them before target position and another one afterwards. They are foreseen to help operators focussing the beam on the scattering target and for driving the beam all the way through the exit of the chamber.

The S1 system placed at the entrance of GLORIA has a rotary cylindrical frame with three circular collimating holes of 20 mm, 15 mm and 8 mm diameters, respectively. At a distance of 225 mm downstream there is the S2 system. It is made of a rectangular frame with collimating holes of 1 mm, 5 mm, 10 mm and 30 mm diameters. At the same frame centred over the 1 mm hole, there is a standard single-pad detector of 500 um thickness (PIP) from CANBERRA [10]. S2 can be both rotated and displaced vertically, so that for beam tuning it is possible to choose among the three collimators, the 1 mm diameter collimator covering the silicon detector or, by rotating the frame, the full detector area of 2 cm diameter.

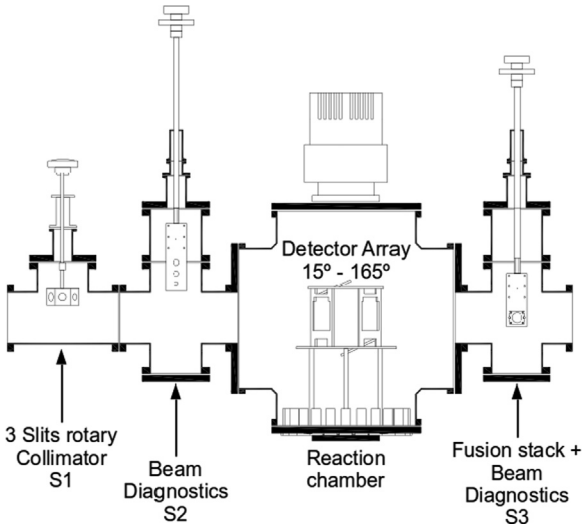

Fig. 2. Sketch of the reaction chamber of GLORIA array including beam-tuning elements. See the text for explanation.

The target holder is placed 355 mm from S2, having room for five different target foils of 2 cm diameter and a Faraday Cup (FC) at the end. It is provided with a push-pull and free rotary system for alignment and positioning. The S3 system is placed 255 mm from reaction target. It consists of a rectangular frame with a 1 mm diameter hole, covering a PIP detector in similar manner as in S2. It also holds a FC with the additional possibility of installing a secondary reaction target (fusion target) for simultaneous measurement of activation cross-sections.

By adjusting the collimators placed at S1, S2 and S3 the beam operator can tune the pilot beam and check the beam size and divergence. By setting the S1 opening at 8 mm and the S2 opening at 5 mm, the operator can optimize beam intensity using the FC placed at the target frame. This configuration would correspond to a beam divergence below 1° and a maximum spot size of 4 mm at target position. Fine alignment of the pilot beam is provided by the FC at S3. By measuring the FC yield at S2 and S3 for each of the collimators at S1 and S2, the beam size at target position can be deduced. In this way the transmission and alignment of the beam can be optimized.

For tuning the radioactive beam, the beam intensity must be reduced until it reaches a value representing no risk for the PIP detectors. This depends on the ionization produced by the beam on the detector [10]. In our case a safe limit adopted for the low energy heavy-ion beams is ~ 1 kHz/cm^2, which is also easily handled by the data acquisition system. When using the pilot beam this counting rate can be achieved without modifying the beam transport parameters, by reducing the intensity of the ion source or, in most cases, by using pepper pots. When the signal is lost at the FC, the PIP detector at S2 can be set facing the beam protected by the 1 mm collimator. By further reduction of the beam intensity S2 can be rotated so the full active area of the PIP detector can face the beam. In this way a direct measurement of RIB intensity and energy is performed. By using the corresponding collimated PIP detector at S3, the RIB beam is driven through the exit of the chamber. Rotating S2 and S3, PIP detectors can be both set to face the beam, and by combining collimators at S1 and S2, the size and divergence of the RIB can be obtained.

4. Front End Electronics (FEE), data acquisition system (DACQ) and control

Each DSSSD detector generates a total of 32 charge signals to be amplified, shaped and digitalized. Including the two PIP detectors for beam tuning, we obtain a total of $12 \times 32 + 2 = 386$ electronic channels from the complete GLORIA detection system. This rather large number of channels can still be handled by using commercially available multipurpose modules.

Front End Electronics (preamplifiers and shapers) have been manufactured by Mesytec GmbH [11]. Junction and ohmic strips of the DSSSD detector (16 strips per side) are connected to a 16-channel preamplifier boards model MPR-64. The preamplifiers are located as close as possible to the reaction chamber in order to improve signal-to-noise ratio. Straight afterwards, energy signals are shaped and amplified using STM-16 modules, which also provide the corresponding trigger for the logic chain when the shaped amplitude exceeds a programmable threshold level. Detectors are biased with a four-channel bias modules model MHV4. PIP detectors signals used for the beam tuning process are amplified and shaped at MSI8 module.

The slow control of the complete system (shaper gains, thresholds, detector bias, etc.) can be remotely operated with a dedicated application [12] implemented within LabVIEW programming

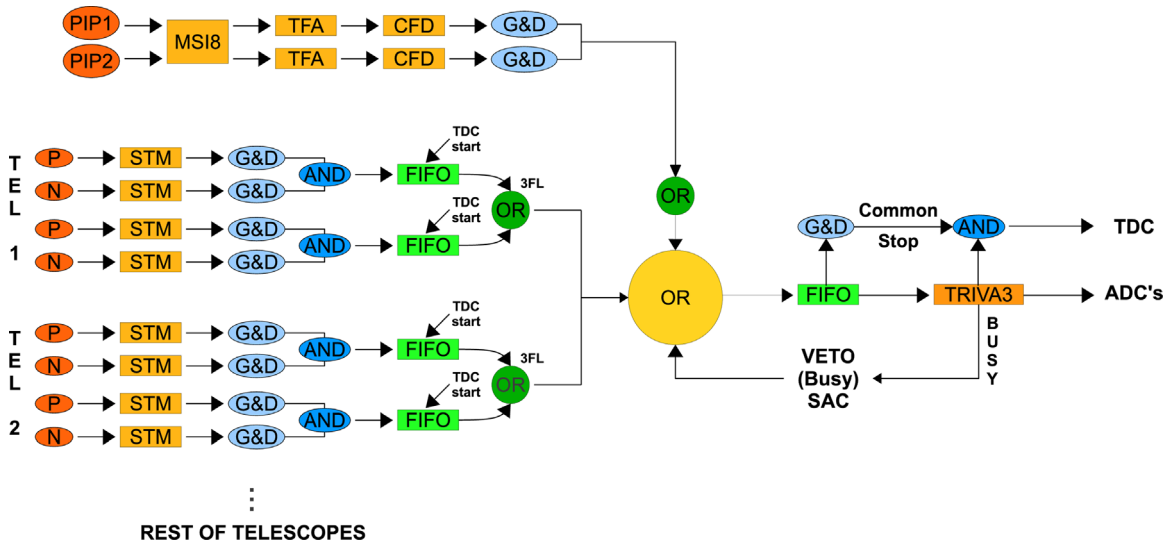

Fig. 3. Trigger setup of GLORIA detector array. TEL(n): DSSSD telescope; P/N: DSSSD junction/ohmic side; PIP 1-2: Silicon detectors for beam diagnostics; MSI8: preamplifier & shaper module; STM: STM16 module; G&D: gate-and-delay; AND/OR (3FL): Triple 4-Fold-logic unit in coincidence/sum; FIFO: Fan-in Fan-Out; TFA: Time-fast-amplifier; CFD: Constant fraction discriminator; ADC: Analogue-to-digital converter; TDC: Time-to-digital converter; TRIVA3: Trigger module; SAC: System acquisition. See the text for explanation.

environment [13] by means of RS232 connection ports linked in a daisy chain.

Data acquisition is based on VME standard cards, most of them manufactured by Caen SpA [14]: peak-sensing analogue-to-digital converters (mod. V785), time-digital-converters (mod. V778) and digital counters/latching-scaler (mod. V830). All these cards are daisy-chained connected and fired simultaneously by the MAIN-TRIGGER (see Fig. 3). This trigger is also used for starting the analogue-to-digital conversion, the time-to-digital conversion process, and the general system data readout. Crate control and trigger management are performed by means of a power PC card model RIO2 from Creative Electronic Systems (CES) [15] running LYNX-OS system and the TRIVA trigger card developed at GSI [16].

Trigger logic is organized in NIM standards via multipurpose modules, also from Caen SpA: Fan-In-Fan-Out (mod. N454), Dual-Timer (mod. N93B), Constant-Fraction discriminator (mod. N843) and Triple 4-Fold Logic Unit (mod. N405). Trigger signals are individually synchronized by using gate-and-delay GG8020 from ORTEC [17].

GLORIA detector will typically run in the so-called coincident-XY TOTAL-OR, configuration, that is, for any DSSSD, all events presenting signal-over-threshold *at ohmic and junction strips* will be accepted for firing the MAIN-TRIGGER of the data acquisition. The coincident-XY condition, implemented at hardware level, becomes very useful for rejecting unphysical events originated from electronic noise. Nevertheless, the flexibility of the hardware configuration foreseen for trigger management makes possible implementing more restricted options.

The schematics of data flow and trigger organization is shown in Fig. 3. After pulse arrival, the constant-fraction gate produced at each STM module (total sum of the 16 strips) is used as a trigger signal. At the first trigger level ohmic vs. junction event coincidence (coincident XY condition) is required for each DSSSD detector. The minimum resolving time of the ohmic/junction coincidence in the electronic chain is 3 ns, which is the limit of the coincidence module (N405). This value matches properly the 3 ns jitter expected to form the gate & delay unit GG8020 and the leading edge resolution of 0.4 ns of the STM-16 module. When coincident events arrive a gate of 25 ns is produced for building the corresponding trigger.

First level triggers are summed to generate a COMMON-OR using another N405 box (the module contains three four-channel logic units with veto), which constitutes the MAIN-TRIGGER used for firing the data acquisition system. The VETO option is used for blocking the readout process when MAIN-TRIGGER is generated as explained below. A similar procedure is envisaged for the two PIP detectors. In this case the fast timing output of the MPR module is first amplified by using N979 module from Caen SpA, and the trigger is generated after filtering with the N843 Constant-Fraction module.

The MAIN-TRIGGER is send simultaneously to the TRIVA module and to a Dual-Timer, the latter used for adjusting the gate width needed for the analogue-to-digital conversion. The TRIVA module initiates the acquisition process and generates the SYSTEM-BUSY gate signal, which is send to block the arrival of signals by vetoing the system COMMON-OR. This gate protects the acquisition during event readout and data processing. A more detailed description of the system will be published elsewhere [18].

Timing measurements are performed using the so-called common-stop method. First-stage (coincident *X*–*Y*) detector-triggers are sent as starting signal for the time-to-digital converter (TDC). The time measurement stops at the arrival of the MAIN-TRIGGER, which is properly delayed by using a gate-and-delay unit to allow all relevant events reaching the acquisition system in time. The TDC module can be operated with a maximum time resolution of 140 ns distributed in 4096 channels (0.03 ns/channel).

Data acquisition software is based on the so-called Multi Branch System (MBS) and Go4 developed at GSI [19,20]. A dedicated PC connected via Ethernet is used for communication with RIO2 and for data storage. Table 1 summarizes the pulse shaping modules, logic and VME cards included in GLORIA front-end, trigger and data acquisition systems.

5. Monte Carlo simulations

Monte Carlo simulations were performed by means of GEANT4 [21–23] and the NPTool packages [24]. The complete geometry of GLORIA including the target ladder and the six DSSSD two-stage

Table 1
Summary of pulse shaping modules, logic and VME cards used for GLORIA silicon detector array.

Unit type	Modules (× channels)	Model	Supplier
Preamplifier	6 (×64)	MPR64	Mesytec GmbH
Detector bias	3 (×4)	MHV4	Mesytec GmbH
Shaper	12 (×16)	STM16	Mesytec GmbH
Preamplifier & Shaper	1 (×8)	MSI8	Mesytec GmbH
Fan-in-fan-out	4 (×4)	N454	Caen SpA
Dual-timer	2	N93B	Caen SpA
Triple 4-fold logic	6 (×3)	N405	Caen SpA
Constant-fraction Discriminator	2	N843	Caen SpA
Fast-amplifier	2	N979	Caen SpA
Gate & delay	8 (×3)	GG8020	Ortec
Crate controller	1	RIO2	CES
Trigger manager	1	TRIVA	GSI
Digital counter/scaler	1 (×32)	V830	Caen SpA
Analogue-to-digital converter	13 (×32)	V785	Caen SpA
Time-digital converter	6 (×32)	V775	Caen SpA
Slow control	1 (×2)	MRC1	Mesytec GmbH

detector telescopes was implemented. For a first analysis of the detector response we have used a simple event generator producing light-ions at target position (1 mg/cm^2 ^{208}Pb). For the energy distribution we have chosen a Gaussian shape with a large width to cover a wide range of energies. The distribution is centred at 15, 20, 24, 40, 48 and 55 MeV for He, Li, Be, B and carbon isotopes respectively. For the purpose of this work a large energy spread (FWHM) of 40% has been chosen in order to provide a better location of the mass region occupied by each isotope. The ion distribution was also a Gaussian shape with parameters adjusted to reproduce typical values of the beam spot (sigma values of 3 and 6 mm diameter) and emittance of $\sim 1\,\pi$ mm mrad.

We have used energy resolution values of 40 KeV and 30 keV for the ΔE and E detectors, respectively. The uniformity of silicon wafer can play an important role in the results of the simulation, mainly for the thin transmission detector DE ($\sim$40 μm) with an active area of 50×50 mm^2. However detector manufacturer guaranteed a thickness uniformity better than 5% for the full silicon wafer, and as the pixel size is only 3×3 mm^2, the quoted level of detector inhomogeneity is not expected to produce a significant effect in a pixel-by-pixel analysis.

A bi-dimensional spectra ΔE vs. E_{total} for the central pixel of the forward DSSSD telescope at 21° is shown in Fig. 4. The banana-like regions correspond to various test isotopes from H to ^{13}C. The hydrogen isotopes show the typical back bending due to the particle punch-through effect at the second stage of the telescope.

The quality of the mass discrimination achieved by a particle detector system can be accounted for by using the "Figure of Merit (FoM)", as defined in [25,26]:

$$\text{FoM} = dEc/(\text{FWHM}_1 + \text{FWHM}_2) \quad (1)$$

being δEc the separation energy between the two adjacent peaks, FWHM_1 and FWHM_2 the corresponding full widths at half-maximum. A detector system will exhibit good identification capability when FoM > 0.7.

We have studied the value of the FoM for the most challenging case of the carbon isotopes. In Fig. 4 we show the projection of an energy slice of this mass region onto the DE axis, centred at 55 MeV and an energy width of 100 keV (red square). The resulting DE energy spectrum is shown in Fig. 5. The distribution has been analysed using a two-Gaussian fit and the result is shown with a blue line. For the present case we obtain a value of FoM=0.9 for ^{12}C/^{13}C identification. It should be noticed that in

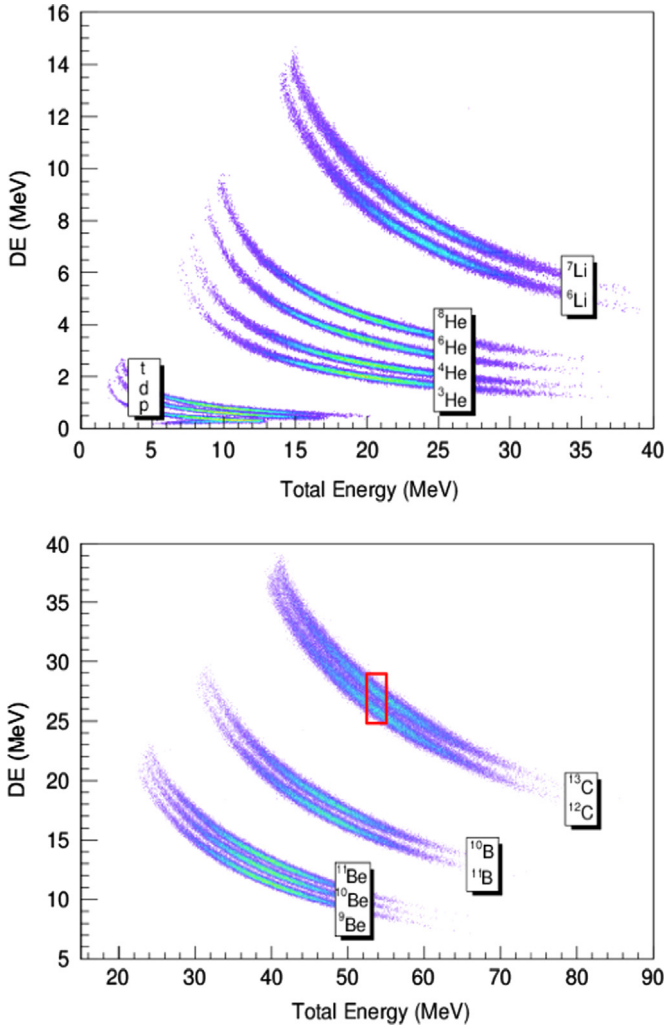

Fig. 4. Monte Carlo simulation of detector response using light ions. In the pictures it is shown the expected mass spectrum obtained at the central pixel (21° Lab) of a forward DSSSD telescope. The region marked with a red square has been used for evaluating the mass resolution (FoM) of the instrument. See the text for explanation. (For interpretation of the references to colour in this figure legend, the reader is referred to the web version of this article.)

routine data analysis a better isotope separation can be expected by the use of dedicated polygonal cuts, or with a suitable mathematical transformation (rotation) of variables [27].

In Fig. 6 we show the simulated geometrical efficiency of the detector array, defined as the ratio between emitted and detected particles, as a function of the observation angle. The angular overlap between DSSSD detectors is around 10° and the simulations confirm that the array can provide a full angular coverage from 15° to 165°. The overlapping angular regions between DSSSD telescopes are localized as a sudden increase in the geometrical efficiency around 15–52° (forward and top detectors), 82–98° (top and bottom detectors) and 128–165° (bottom and backward detectors). Pixel solid angles vary between 2.0 and 2.5 msr along a given telescope.

6. First experimental results with exotic beams

The detection system GLORIA was commissioned in October 2010 in the SPIRAL ISOL facility at the Grand Accelerateur National D'Ions Lourds (GANIL) in Caen, France [28]. A radioactive ion beam of ^{8}He at energies of 16 and 22 MeV (Lab) was used to study the

dynamics of the system ^{8}He+^{208}Pb at energies around the Coulomb barrier [29].

The $^{8}He^{1+}$ beam was produced by fragmentation reactions induced by a 75 MeV/nucleon ^{13}C beam impinging on a thick graphite target. The beam was purified and reaccelerated at the CIME cyclotron up to 2.0 and 2.75 A MeV, with an energy resolution $\sim 10^{-3}$. Afterwards the beam was driven trough the GANIL accelerator complex up to the G21 experimental area, where the GLORIA array had been setup.

A self-supported ^{208}Pb reaction target of 1 mg/cm^2 thickness was used for the experiment. A beam spot size of 4 mm and an average intensity of 5×10^5 pps were measured at target position (S2). A low-rate pulse-generator test signal was also used for monitoring the behaviour of the electronic chain and the dead time of the data acquisition system.

Energy calibration of the detectors was carried out in a pixel-by-pixel basis by using a triple alpha source (^{239}Pu, ^{241}Am and ^{244}Cu) and the corresponding ^{8}He elastic peak. A different procedure was used for DE and E detectors according to the energy range of the reaction fragments to be detected. Corrections for energy losses in the target and detector dead layers were also taken into account.

The energy calibration of the DE detector was obtained by using the triple alpha source, as the energy loss of the relevant reaction fragments was expected to be around 5 MeV. No dead layer correction was needed in this case as irradiation was performed directly on the junction side, which is also windowless, as the usual Aluminium metallization layer is replaced by an open grid [30].

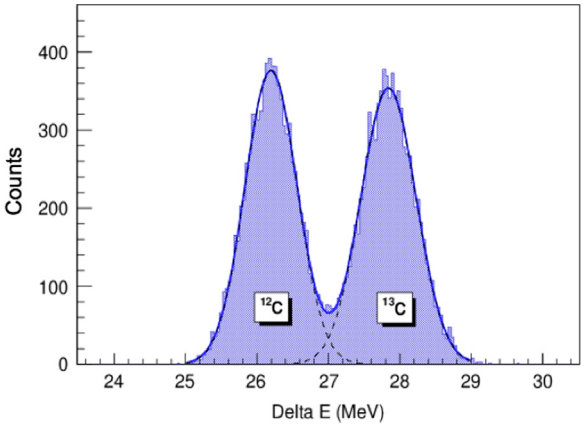

Fig. 5. Projection of an energy slice of the carbon mass region onto the DE axis centred at 55 MeV and an energy width of 100 keV. See the text for discussion.

The E detector should cover much wider energy range, up to ~15 MeV, and therefore the calibration was performed with both triple alpha source and the corresponding elastic peak. The energy calibration was first carried out by irradiation of the ohmic side with the triple alpha source. This side could introduce significant energy losses due to the usual Aluminium metallization and undepleted silicon layers. Corrections were introduced by optimizing the constant coefficient of the linear calibration equation in order to reproduce the energy of the elastic peak. To obtain the energy of the elastic peak the procedure was the following. For each angle, we calculated the expected energy of elastic events after passing through the lead target (1.0 mg/cm^2) and the DE detector. The energy loss at the target was obtained from a SRIM [31] simulation assuming that elastic events were produced at half the target thickness. The energy loss due to the DE detector was obtained directly from the measured data (note that DE was calibrated previously) by fitting the energy distribution corresponding to the elastic events. We obtained a typical energy resolution of 30 keV for the DSSSD detectors (FWHM), and of about 100 keV for the telescopes. This is roughly 0.5% of elastic peak energy and altogether with this procedure we obtained a slightly better value than previous works reported in the literature [4,32,33] for similar beams and energies using silicon strip detector telescopes.

A typical particle identification spectrum of the forward telescope at 22 MeV is shown in Fig. 7. The simulated Monte Carlo spectrum is superimposed using grey dots, showing good agreement with the measurements. This data corresponds to the sum of all pixel events, calibrated in energy, with the same observation angle centred at 25° Lab. By using this representation it is possible to identify the different isotopes produced in the reaction, relevant reaction channels and also to analyse the response of the detector system. Events corresponding to the elastic channel and ^{6,4}He production are clearly separated as predicted by our Monte Carlo calculations. The weak group of ^{8}He ions located at the left side of the main ^{8}He peak can be attributed to the excitation of ^{208}Pb to its first 0+ state at E_{ex}= 2.61 MeV. In addition to the elastic peak, a low energy region appears with constant total energy but decreasing DE, which is a consequence of channelling in the DE detector.

On the other hand, there is a group of events below the elastic peak, close to the expected ^{6}He region and surrounded by a red circle, which can be attributed to incomplete charge collection effects at inter-strip sites due to the grid structure of DSSSD detector [34]. The observed energy shift of about ~1 MeV can be seen more clearly in the DE vs. E spectrum shown in Fig. 8 (red circle). These events belong to the elastic channel and deposit the expected energy in the E detector, but the signal recorded on the DE counter is systematically smaller. Similar effects were reported

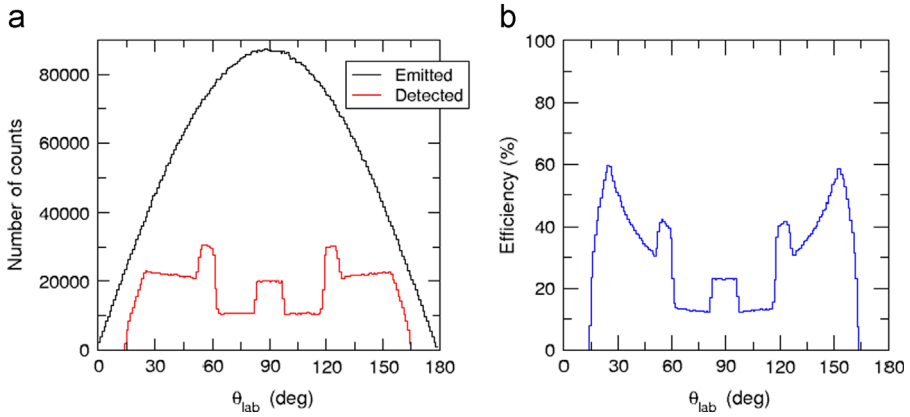

Fig. 6. Left: the angular distribution of the emitted particles produced by the event-generator is shown with a black solid line, whereas the corresponding distribution of the detected particles is shown with a red line. Right: angular distribution of the geometrical efficiency. See the text for discussion. (For interpretation of the references to colour in this figure legend, the reader is referred to the web version of this article.)

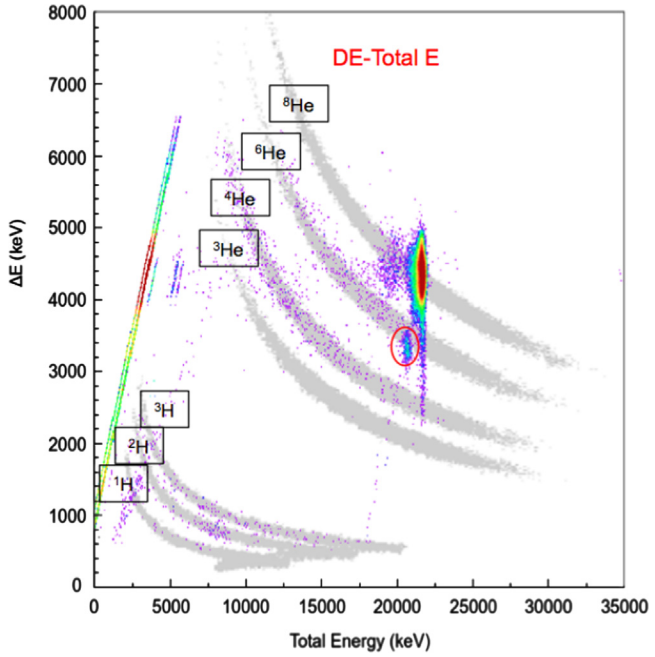

Fig. 7. Comparison between simulated and experimental data for the reaction ^{8}He+^{208}Pb at 22 MeV, for a forward telescope, at the observation angle of 25° (Lab). The grey dots were generated with NPTools package while the coloured dots corresponds to the experimental data. See the text for discussion. (For interpretation of the references to colour in this figure legend, the reader is referred to the web version of this article.)

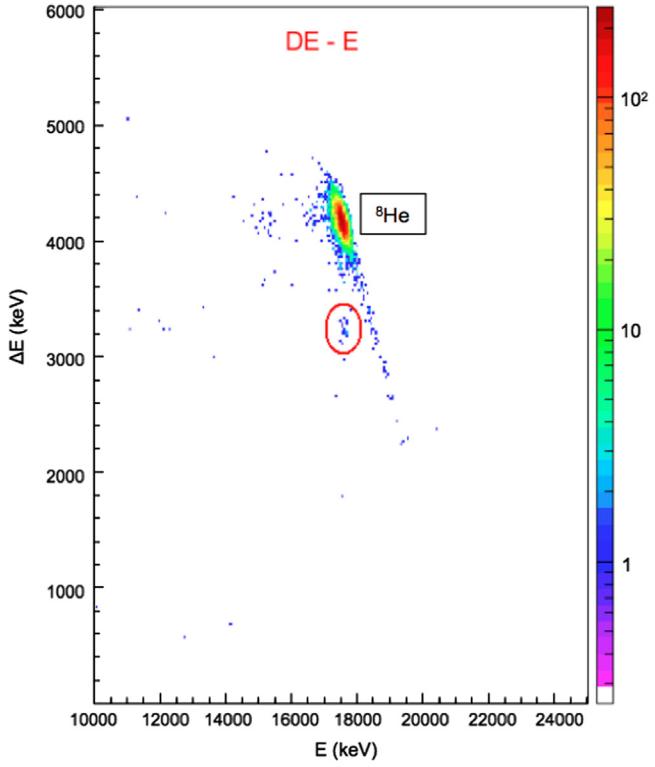

Fig. 8. Spectrum of DE vs. E for a single pixel for the reaction ^{8}He+^{208}Pb at 22 MeV, for a forward telescope, at the observation angle of 25° (Lab). A red circle is marked over observed inter-strip events. See the text for discussion. (For interpretation of the references to colour in this figure legend, the reader is referred to the web version of this article.)

in Refs. [4,35,36]. This phenomenon depends on beam energy and it is produced by an incomplete charge collection on the inters-trip region of the ΔE detector, which results in a reduced pulse height.

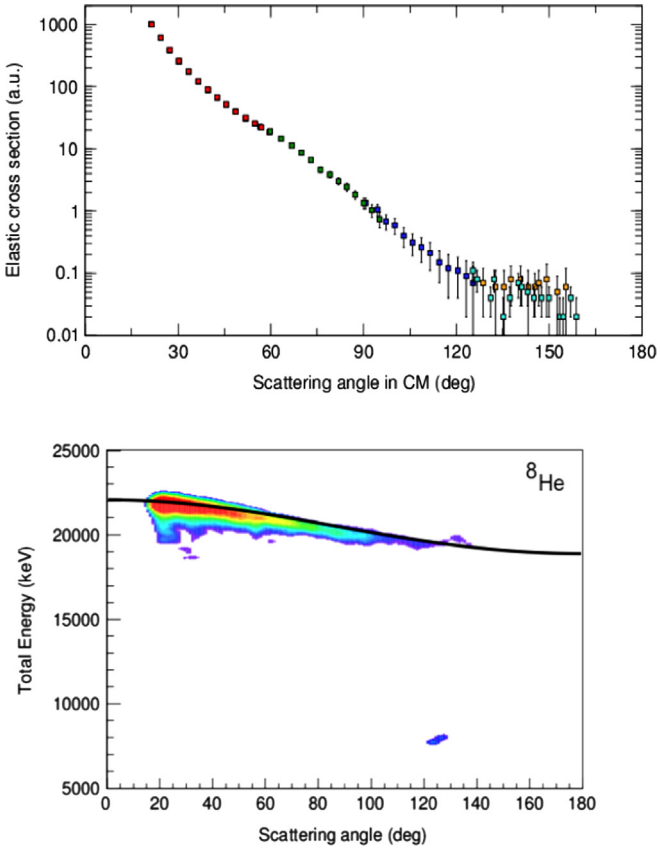

Fig. 9. Top: preliminary angular distribution of elastic cross-sections (arbitrary units). Red and purple dots correspond to the forward telescopes of GLORIA, green and blue to the upper and bottom telescopes, light-blue and yellow dots to the backward telescopes, respectively. Bottom: distribution of total energy vs. angle for ^{8}He mass region at scattering angle of 25° (Lab). The black solid line shows the calculated elastic channel kinematics. See the text for discussion. (For interpretation of the references to colour in this figure legend, the reader is referred to the web version of this article.)

In contrast to the channelling events identified above, there is no corresponding increase in the measured E-signal. Altogether it accounts for less than 1% of elastic events, and they can be separated from the relevant reaction channels during the off-line analysis. Incomplete charge collection effects are also present in the ^{8}He mass region, along the tail of the elastic peak. They are weakly shown in Figs. 7 and 8 due to the off-line analysis process, where it required an energy coincidence (<300 keV) between junction and ohmic energy signals (X-Y) at DE detector for cleaning the spectra.

A preliminary angular distribution of the elastic cross-sections is shown in Fig. 9 (Top), where data points obtained from the six telescopes are plotted with different colours. Scattering angles were obtained by using Monte Carlo simulations, taking the centre of the corresponding ion distribution registered at each single pixel. Good matching is found between the six telescopes of GLORIA, providing a smooth and continuous angular distribution from 15° to 160° (CM). In Fig. 9 (Bottom) we show the total energy of the events corresponding to the ^{8}He mass region as a function of the scattering angle. We should note that the distribution includes a small fraction of events due to ^{208}Pb excitation. The experimental result agrees with the expected energy angular dependence of the elastic scattering, which is shown with a black solid line.

Similar analysis was performed for the ^{6}He and ^{4}He isotopes. For each mass region, the corresponding energy vs. detection angle is shown in Fig. 10. Regions attributed to neutron transfer to

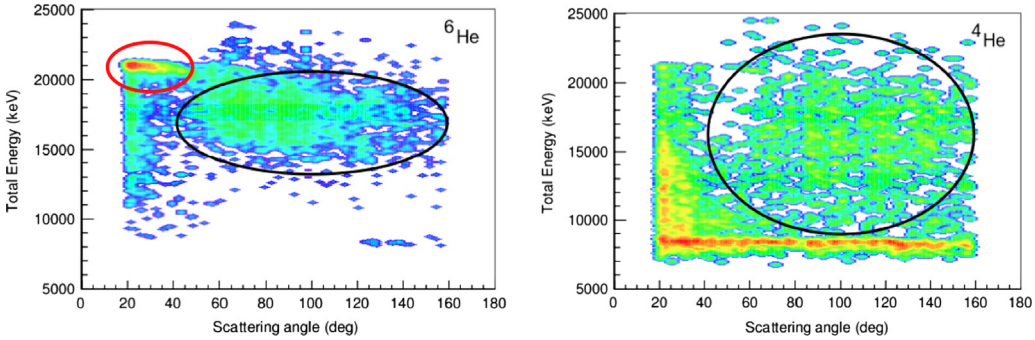

Fig. 10. Left: plot of energy vs. observation angle for events in the mass region corresponding to ^{6}He for the full GLORIA array. Neutron transfer events are identified inside the area surrounded with a black solid line, clearly separated from the rest. Events due to incomplete charge collection due to ^{8}He (and not ^{6}He) are surrounded with a red solid line. Right: Same plot as before for events in the mass region corresponding to ^{4}He. See the text for discussion. (For interpretation of the references to colour in this figure legend, the reader is referred to the web version of this article.)

the continuum, as expected from Coupled Channel Calculations [37], have been surrounded with a black solid line. In the case of ^{6}He, the region previously identified as incomplete charge collection of ^{8}He events can be clearly observed in the upper part of the spectrum at very forward angles (red circle). The lower part of Fig. 10 (Right) shows the production of ^{4}He arising from fusion-evaporation which is nicely separated from the rest of reaction channels forming a uniform straight line. Data analysis of this experiment is still in progress and the results will be published elsewhere.

7. Summary and conclusions

The development of new radioactive beam facilities provides unique opportunities for performing nuclear reaction studies. The usually low intensities available at these facilities will benefit from the use of high granularity and large solid angle detector arrays.

In this paper the design and construction of a new charged particle detector system (GLORIA) has been described for measuring heavy-ion reactions induced by exotic nuclei at energies around the Coulomb barrier. It is a compact silicon array of reduced size based on the use of two-stage DSSSD detector telescopes of 40 μm and 1 mm silicon thickness, respectively. The geometry has been optimized to cover an angular range of 15–160° (Lab), maintaining an overlap of 10° between adjacent telescopes. An angular resolution of $\pm 2.5^{\circ}$ (Lab) can be achieved by using 3 mm pitch strip detectors placed at 60 mm from reaction target. The rotated target configuration allows for measuring angular distributions of reaction quantities at angles around 90° (Lab).

A dedicated Monte Carlo simulation programme based on NPtool and GEANT4 packages has been implemented and put into operation. The simulations predict the capacity of GLORIA to separate light reaction fragments up to carbon isotopes at low collision energies.

Data acquisition and trigger system have been implemented by using commercial highly integrated front-end electronics and VME standards. The slow control system is based on LabVIEW whereas the data acquisition and monitoring systems have been implemented on MBS and Go4 systems developed at GSI Laboratory (Darmstadt, Germany).

The GLORIA detector array was first commissioned at the SPIRAL facility at the Grand Accelerateur National D'Ions Lourds (GANIL) for the study of the system ^{8}He+^{208}Pb at energies around the Coulomb barrier. The array has demonstrated the predicted isotope separation capability up to Helium isotopes, in good agreement with Monte Carlo simulations. It was also possible to obtain continuous angular distributions of relevant physics quantities in a wide angular range from 15° to 160° (Lab) with an acceptable energy resolution of about 100 keV. The reaction mechanisms can be identified by the combination of the mass separation, energy and angular distributions.

Unfortunately the reaction system ^{8}He+^{208}Pb at 22 MeV does not produce significant yields of reaction fragments above Helium, and with present data we cannot prove mass separation for heavier isotopes. New experiments are foreseen with GLORIA detector where it will be possible to develop a competitive programme on low energy reactions with exotic nuclei, and to test mass separation capability up to the design goal, the carbon isotopes.

Acknowledgements

This work was supported in part by the Grant FPA2010-22131-C02-01 (FINURA) from the Spanish Ministry of Economy and Competitiveness, Grant N202 033637 from the Ministry of Science and Higher Education of Poland, Grant VH-VI-417 from Helmholtz Association in Germany, and Contract EUI2009-04163 (EUROGENESIS) from the European Science Foundation.

References

[1] Yu. E. Penionzhkevich, Physics of Atomic Nuclei 71 (2008) 1127.
[2] A. Bonaccorso, Physica Scripta T152 (2013) 014019.
[3] ⟨http://www.micronsemiconductor.co.uk/products-strip.asp?productsubcatID=1⟩, 2014.
[4] Y. Blumenfeld, et al., Nuclear Instruments and Methods A 421 (1999) 471.
[5] E. Pollaco, et al., European Physics Journal A 25 (s01) (2005) 287.
[6] M. Labiche, et al., Nuclear Instruments and Methods A 614 (2010) 439.
[7] F. Azaiez, W. Korten, Nuclear Physics News 7 (1997) 21.
[8] E. Farnea, et al., Nuclear Instruments and Methods A 621 (2010) 331.
[9] C. Schmitt, et al., Nuclear Instruments and Methods A 621 (2010) 558.
[10] ⟨http://www.canberra.com/products/detectors/pips-detectors-particle-identification.asp⟩, 2013.
[11] ⟨http://www.mesytec.com⟩, 2013.
[12] D. Cruz et al. Sistema de Control de Parámetros Lentos de un Sistema de Detección de Partículas Cargadas (Master thesis), University of Huelva Huelva, Spain, 2010. Unpublished.
[13] ⟨http://www.ni.com/labview/esa/⟩, 2014.
[14] ⟨http://www.caen.it/csite/Product.jsp?parent=11&Type=Product⟩, 2014.
[15] ⟨http://www.ces.ch/technology/backward-compatible⟩, 2010.
[16] H.G. Essel, N. Kurtz, IEEE Transactions on Nuclear Science NS-47 (2000) 337.
[17] ⟨http://www.ortec-online.com/download/GG8020.pdf⟩, 2010.
[18] G. Marquínez-Durán, (Ph.D. thesis), University of Huelva, Spain. In preparation.
[19] ⟨http://www-win.gsi.de/daq⟩, 2010.
[20] ⟨http://www-win.gsi.de/go4⟩, 2013.
[21] S. Agostinelli, et al., Nuclear Instruments and Methods A 506 (2003) 250.
[22] J. Allison, et al., IEEE Transactions on Nuclear Science NS-53 (2006) 270.
[23] ⟨http://geant4.cern.ch⟩, 2014.
[24] ⟨http://gaspard.in2p3.fr/simu.html⟩, 2011.
[25] R.A. Winyard, et al., Nuclear Instruments and Methods 95 (1971) 141.
[26] A. Van Oosterom, et al., IEEE Transactions on Biomedical Engineering 30 (1983) 125.
[27] S. Barlini, et al., Nuclear Instruments and Methods A 600 (2009) 644.

[28] A.C.C., Nuclear Physics A 693 (2001) 465.
[29] I. Martel and K. Rusek, Proposal to GANIL PAC. Experiment E587S, 2008.
[30] O. Tengblad, et al., Nuclear Instruments and Methods A 525 (2004) 458.
[31] J.F. Ziegler, P. Biersack, U. Littmark, in: J.F. Ziegler (Ed.), The Stopping and Range of Ions in Matter, Pergamon, New York, 2008 (See also).
[32] A. Sánchez-Benítez, et al., Nuclear Physics A 803 (2008) 30.
[33] A. Lemasson, et al., Physical Review C 82 (2010) 044617.
[34] O. Tengblad, et al., Nuclear Instruments and Methods A 525 (2004) 458.
[35] C. Diget, et al., Journal of Instrumentation 6 (2011) P02005, http://dx.doi.org/10.1088/1748-0221/6/02/P02005.
[36] D. Torresi, et al., Nuclear Instruments Methods A 713 (2013) 11.
[37] K. Rusek and N. Keeley. Private Communication.